A Unity Bit Coding Method by Negative Feedback*

HIROSHI INOSE†, MEMBER, IEEE, AND YASUHIKO YASUDA‡

Summary—**Signal-to-noise performances of a unity bit coding method and the characteristics of an experimental video encoder based upon the principle are described. The system contains a signal integration process in addition to the original delta modulator and features capability of transmitting dc component of input signal.**

The characteristics of the quantizing noise to the signal frequency, the signal amplitude and the integrator time constant are obtained theoretically as well as experimentally. The characteristics of periodical noise which are inherent to the proposed system are also investigated.

The design and the characteristics of an experimental encoder for digital transmission of video signals are described as examples of the experimental equipment constructed to demonstrate the realizability of the principle. The experimental results show that considerably good reproduction of video pictures is obtained with sampling frequency as low as 30 Mc and suggest that the proposed system well fulfills the purpose.

PRINCIPLE

DELTA MODULATION, characterized by simpler circuitry as compared with PCM, not always fulfills the purpose of digital transmission of signals. This is due to the fact that the output of the delta modulator carries the information which is the differentiation of the input signal. In other words, it is incapable of transmitting dc component, its dynamic range and SNR are inversely proportional to the signal frequency[1] and the inevitable integration at the receiving end causes an accumulative error when the system is subject to transmission disturbances. Consequently, delta modulation has been intended mainly for the transmission of such signals as speech which does not contain dc component and has less energy in higher frequencies. It has been felt that a different approach may be preferable for the transmission of telemetering signals, video signals and the like which generally have rather uniform frequency spectra with dc component, and for the transmission of signals through adverse transmitting conditions.

A modification of delta modulation has been proposed[2] to meet the requirements. To compensate for the inevitable differentiation of the input signal, the proposed system has a signal integration process added at the input of original delta modulator as is shown in Fig. 1. The input to the pulse modulator $\epsilon(t)$ is the difference of the integrated input signal $\int s(t)dt$ and the integrated output pulses $\int p(t)dt$ so that $\epsilon(t)=\int s(t)dt-\int p(t)dt$. For the realization of this original configuration, an integrator with infinite dynamic range is needed. However, since the subtraction is a linear process, the above equation of $\epsilon(t)$ is rewritten as $\epsilon(t)=\int\{s(t)-p(t)\}dt$ so that the two integrators can be combined and replaced as shown in Fig. 2. In this modified configuration, the input to the integrator is the difference signal $\{s(t)-p(t)\}$ which stays within a certain limit if the system operates properly, and hence the integrator is practically realizable.

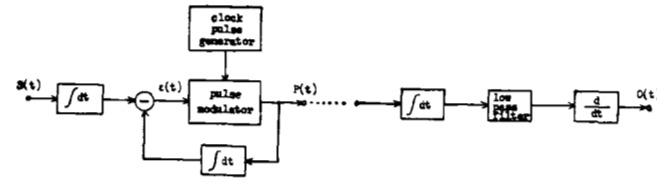

Fig. 1—Block diagram of a modified delta modulator.

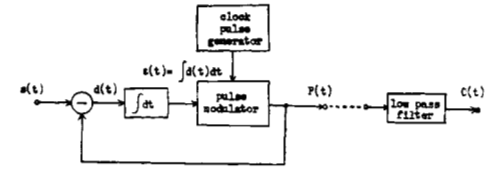

Fig. 2—Block diagram of the system.

The configuration of Fig. 2 has been named as $\Delta-\Sigma$ modulation and has been described with particular reference to the digital telemetering.[2] In the figure, the output pulses $p(t)$ are fed back to the input and subtracted from the input signal $s(t)$ which varies sufficiently slower than the sampling pulses. The difference signal $d(t)=s(t)-p(t)$ is integrated to produce $\epsilon(t)=\int d(t)dt$ and enters the pulse modulator. The pulse modulator compares the amplitude of the integrated difference signal $\epsilon(t)$ with a predetermined reference level and opens the gate to pass a pulse from the pulse generator when $\epsilon(t)$ is larger than the reference level and closes the gate to inhibit the pulse when $\epsilon(t)$ is smaller than the reference level. Through this negative feedback procedure, the integrated difference signal is always kept in the vicinity of the reference level of the pulse modulator, provided that the input signal is not too large. Hence if the amplitude of the input signal becomes large, the output pulses appear more frequently In other words, the output pulses carry the information corresponding to the input signal amplitude. Demodula-

* Received July 24, 1963. Partly presented at the International Telemetering Conference, London, England; 1963.

† Faculty of Engineering, University of Tokyo, Japan.
‡ Institute of Industrial Science, University of Tokyo, Japan.

[1] F. de Jager, "Delta modulation—a method of PCM transmission using the one unit code," *Philips Res. Repts.*, vol. 7, pp. 442–466; 1952.

[2] H. Inose, Y. Yasuda, and J. Murakami, "A telemetering system by code modulation—$\Delta-\Sigma$ Modulation," IRE TRANS. ON SPACE ELECTRONICS AND TELEMETRY, vol. SET-8, pp. 204–209; September, 1962.

tion in the receiving end is performed by reshaping the received pulses and passing them through a low-pass filter. Since no integration process is involved in the demodulation, no accumulative error due to transmission disturbances results in the demodulated signal.

The other feature of the system over delta modulation is the input-output characteristic. In the latter, the maximum allowable input signal amplitude that does not overload the system is inversely proportional to the input signal frequency, because the maximum slope of the local-decoder output waveform is constant under the predetermined step voltage and sampling frequency. On the other hand, in the former, the maximum allowable input signal voltage is equal to the product of the amplitude and the duty ratio of the output pulses and therefore is independent to the signal frequency.

The integrator in the forward path is not necessarily a single integrator but may be a double integrator, or more generally, be any signal processing networks favorable to the system performance.

The modulation system may be multiplexed on a time division basis as in other digital modulation systems. However, the pulse pattern of the information channels must be taken into consideration to the frame synchronization.

The frame synchronization pattern generally used in digital communications systems is successive ones. But this pattern in the modulation system is vulnerable because the same pattern appears stationary in the signal channel at the edge of the input dynamic range.

Similarly, such patterns as $\cdots 1010 \cdots$, $\cdots 001001 \cdots$ and $\cdots 110110 \cdots$ may appear stationary. Thus the synchronization pattern should be one of the patterns $\cdots 11001100 \cdots$, $\cdots 111000111000 \cdots$ etc., that do not appear stationary.

In the following sections, the considerations on the signal-to-noise performance of the proposed system as well as the design and the characteristics of an experimental video coder are described.

Signal-to-Noise Characteristics

Quantizing Noise

Fig. 3 shows a generalized block diagram of the system. The modulator output $p(t)$ is fed back to the input and subtracted from the input signal $s(t)$ to produce $d(t)$. The difference $d(t)$ enters a network having the transfer function $A(\omega)$ and comes out of it as $\epsilon(t)$. The network need not necessarily be an integrator. The comparator with characteristics $f\{\epsilon(t)\}$ forwards the sampling pulse $r(t)$ to the output according to $\epsilon(t)$. At the receiving end, the pulse $p(t)$ is fed through a demodulating network having the transfer function $B(\omega)$ and produces the demodulated output $o(t)$. The difference between $s(t)$ and $o(t)$, $n(t)=s(t)-o(t)$ is the error or the

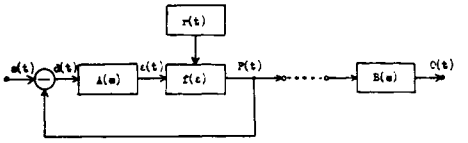

Fig. 3—Generalized block diagram of the system.

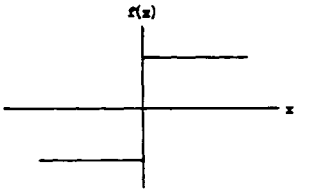

Fig. 4—Characteristic of the comparator.

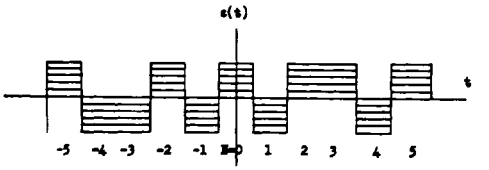

Fig. 5—Assumed waveform of $\epsilon(t)$.

noise of the system. Denoting the frequency domain characteristics of $s(t)$, $d(t)$, $\epsilon(t)$, $p(t)$ and $n(t)$ as $S(\omega)$, $D(\omega)$, $E(\omega)$, $P(\omega)$ and $N(\omega)$, respectively, the frequency domain equations of the system are expressed as

$$D(\omega) = S(\omega) - P(\omega) \tag{1}$$

$$E(\omega) = A(\omega)D(\omega) \tag{2}$$

$$O(\omega) = B(\omega)P(\omega) \tag{3}$$

$$N(\omega) = S(\omega) - O(\omega). \tag{4}$$

Rigorous solution of these equations is impossible since the comparator has such an abrupt nonlinearity as in Fig. 4. Hence, the following assumptions are in order to simplify the treatment.

1) The output pulse $p(t)$ has NRZ (Non-Return-To-Zero) waveform. In other words, the output pulse has the width equal to the sampling period.

2) The error voltage $\epsilon(t)$ is assumed to be rectangular waveforms whose amplitude ranges, with equal probability, from zero to Δ, the peak of the response of the converting network to the output pulse $p(t)$, as shown in Fig. 5. If we assume that the amplitude of the rectangular waveforms is always Δ,

$$\epsilon(t) = \sum_{\lambda=-\infty}^{\infty} \eta_\lambda f(t - \lambda T_r) \tag{5}$$

where T_r is the sampling period and η_λ is expressed by

$$\eta_\lambda = \begin{cases} +1, & \epsilon(t) > 0 \\ -1, & \epsilon(t) < 0. \end{cases} \tag{6}$$

However this obviously overestimates the value since $\epsilon(t)$ results from $d(t)$ which is the difference between

$p(t)$ and $s(t)$. With the assumption that the amplitude takes the value between zero and Δ with equal probability, the power of $\epsilon(t)$ is reduced by the following factor:

$$\frac{1}{\Delta^2}\int_0^{\Delta} y^2 \frac{dy}{\Delta} = \frac{1}{3}. \tag{7}$$

Therefore $\epsilon(t)$ is expressed as

$$\epsilon(t) = \frac{1}{\sqrt{3}} \sum_{\lambda=-\infty}^{\infty} \eta_\lambda f(t - \lambda T_r). \tag{8}$$

3) The demodulating network is assumed to have brickwall low-pass characteristics with cutoff angular frequency of ω_c as

$$B(\omega) = \begin{cases} 1 & |\omega| \leq \omega_c \\ 0 & |\omega| > \omega_c. \end{cases} \tag{9}$$

The Fourier transform of $f(t)$ is expressed as

$$F(\omega) = \Delta T_r S_a\left(\frac{\omega T_r}{2}\right) \tag{10}$$

where $S_a(x) = \sin x/x$. From (8) the Fourier transform of the portion of $\epsilon(t)$ between number $-m$ and m is

$$E_m(\omega) = \frac{\Delta T_r}{\sqrt{3}} \sum_{\lambda=-m}^{m} S_a\left(\frac{\omega T_r}{2}\right) e^{-j\lambda\omega T_r}. \tag{11}$$

From (1), (2) and (9)

$$\begin{aligned} E(\omega)B(\omega) &= A(\omega)\{S(\omega) - P(\omega)\}B(\omega) \\ &= A(\omega)\{S(\omega) - O(\omega)\} = A(\omega)N(\omega). \end{aligned} \tag{12}$$

Hence for the portion between $-m$ and m, the noise is expressed as

$$N_m(\omega) = \frac{B(\omega)}{A(\omega)} E_m(\omega). \tag{13}$$

The power spectrum of the noise is given as

$$\begin{aligned} W_n(\omega) &= \lim_{m\to\infty} \frac{1}{(2m+1)T_r} N_m(\omega) N_m^*(\omega) \\ &= \frac{B(\omega)B^*(\omega)}{A(\omega)A^*(\omega)} \frac{\Delta^2 T_r}{3} S_a^2\left(\frac{\omega T_r}{2}\right) \\ &\quad \cdot \lim_{m\to\infty} \frac{1}{2m+1} \sum_{\lambda} \sum_{\mu} \eta_\mu e^{j(\lambda-\mu)\omega T_r}. \end{aligned} \tag{14}$$

Since the terms

$$\lim_{m\to\infty} \frac{1}{2m+1} \sum_{\lambda} \sum_{\mu} \eta_\lambda \eta_\mu e^{j(\lambda-\mu)\omega T_r}$$

is unity, (14) reduces to

$$W_n(\omega) = \frac{\Delta^2 T_r}{3} \frac{|B(\omega)|^2}{|A(\omega)|^2} S_a^2\left(\frac{\omega T_r}{2}\right). \tag{15}$$

Thus the noise power N^2 within the pass band of $B(\omega)$ is given as

$$N^2 = \frac{\Delta^2 T_r}{6\pi} \int_{-\omega c}^{\omega c} \frac{1}{|A(\omega)|^2} S_a^2\left(\frac{\omega T_r}{2}\right) d\omega. \tag{16}$$

On the other hand, the signal power S^2 when the input signal is sinusoidal is expressed as

$$S^2 = M^2 \frac{h^2}{2} \tag{17}$$

where h is the one half of the dynamic range and M is the ratio between the input signal amplitude and h.

The SNR of the system will be obtained if the characteristics of $A(\omega)$ is given.

Single Integrator: If $A(\omega)$ is characterized by a single integrator of Fig. 6 as

$$A(\omega) = \frac{G}{1 + j\omega\tau} \tag{18}$$

where G is the gain of the amplifier and τ is the time constant CR, the peak of the response to a pulse with amplitude h and duration T_r is

$$\Delta = Gh(1 - \epsilon^{-T_r/\tau}). \tag{19}$$

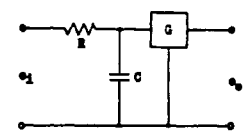

Fig. 6—Single integrator.

Hence

$$|A(\omega)|^2 = \frac{G^2}{1 - \omega^2\tau^2} = \frac{2}{h^2(1 - \epsilon^{-T_r/\tau})^2}. \tag{20}$$

Substituting this into (16),

$$\begin{aligned} N^2 &= \frac{T_r h^2}{3\pi}(1 - e^{-T_r/\tau})^2 = 2 = \\ &\quad \cdot \int_0^{\omega_c} (1 + \omega^2\tau^2) S_a^2\left(\frac{\omega T_r}{2}\right) d\omega. \end{aligned} \tag{21}$$

Since $(\omega T_r/2) \ll 1$, expanding $S_a^2(\omega T_r/2)$ as

$$S_a^2\left(\frac{\omega T_r}{2}\right) = 1 - \frac{1}{3}\left(\frac{\omega T_r}{2}\right)^2 + \cdots$$

and neglecting terms except the first, (21) becomes

$$N^2 = \frac{T_r h^2}{3\pi}(1 - \epsilon^{-T_r/\tau})^2 \omega_c \left(1 + \frac{\omega_c^2\tau^2}{3}\right). \tag{22}$$

Thus the SNR is expressed as

$$\frac{S^2}{N^2} = M^2 \frac{3\pi}{2T_r\omega_c(1-\epsilon^{-T_r/\tau})^2\left(1+\frac{\omega_c^2\tau^2}{3}\right)}. \quad (23)$$

Denoting $1/T_r=f_r$ and normalizing as $2\pi f_r/\omega_c=\alpha$ and $\omega_c\tau/2\pi=\beta$ and rewriting

$$\frac{S^2}{N^2} = M^2 \frac{3\alpha}{4(1-\epsilon^{-1/\alpha\beta})^2\left(1+\frac{1}{3}\pi^2\beta^2\right)}, \quad (24)$$

stability of operation. Therefore the time constant should be chosen to compromise the conditions.

Double Integrator: Fig. 8 shows a double integrator with an interstage amplifier of unity gain which is provided to isolate R_1C_1 and R_2C_2, so that the transfer function is expressed as

$$A(\omega) = \frac{G}{(1+j\omega\tau_1)(1+j\omega\tau_2)} \quad (26)$$

where $\tau_1=R_1C_1$ and $\tau_2=R_2C_2$. If the condition $\tau_1+\tau_2 \gg R_1C_2$ exists, the transfer function of the circuit without the interstage amplifier is approximately the same as (26). Through the similar calculation as in the case of single integration, the SNR is expressed as follows.

$$\frac{S^2}{N^2} = M^2 \frac{3\alpha}{4\left(\frac{1-\epsilon^{-1/\alpha\beta_1}}{1-\gamma}+\frac{1-\epsilon^{-1/\alpha\beta_1\gamma}}{\frac{1}{\gamma}-1}\right)^2\left\{1+\frac{4}{3}\pi^2(1+\gamma^2)\beta_1^2+\frac{16}{5}\pi^4\beta_1^4\gamma^2\right\}} \quad (27)$$

and

$$\frac{S^2}{N^2} = \begin{cases} \frac{3}{4}\alpha M^2 & \text{for } \beta \to 0 \quad (\text{or } \tau \to 0) \\ \frac{9}{16\pi^2}\alpha^3 M^2 & \text{for } \beta \to \infty \quad (\text{or } \tau \to \infty). \end{cases} \quad (25)$$

This means that the SNR is proportional to $(f_r)^{3/2}$ for sufficiently large values of τ. This relationship is similar to that of the delta modulation. However (24) indicates that the SNR is independent of the signal frequency. This is one of the major differences of the system from delta modulation in which both the SNR and the dynamic range are inversely proportional to the signal

where

$$\frac{2\pi f_r}{\omega_c}=\alpha, \quad \frac{\omega_c\tau_1}{2\pi}=\beta_1, \quad \frac{\omega_c\tau_2}{2\pi}=\beta_2 \quad \text{and} \quad \frac{\beta_2}{\beta_1}=\gamma.$$

If $\gamma\to\infty$,

$$\lim_{\gamma\to\infty}\frac{S^2}{N^2} = M^2 \frac{9\alpha^3}{16\pi^2\left(1+\frac{12}{5}\pi^2\beta_1^2\right)(1-\epsilon^{-1/\alpha\beta_1})^2} \quad (28)$$

and if $\gamma\to 1$ (or $\beta_2\to\beta_1$)

$$\lim_{\gamma\to 1}\frac{S^2}{N^2} = M^2 \frac{3\alpha}{4\left\{1-\left(1+\frac{1}{\alpha\beta_1}\right)\epsilon^{-1/\alpha\beta_1}\right\}^2\left(1+\frac{8}{3}\pi^2\beta_1^2+\frac{16}{5}\pi^4\beta_1^4\right)}. \quad (29)$$

frequency. This characteristic enables the system's suitability to signals with rather uniform power spectrum such as in telemetering and video transmission.

Eq. (24) also indicates that the SNR is improved with the increase of α or the sampling frequency f_r, but is maximum with certain value of β or the integrator time constant τ. The results of calculations by Newton's iteration method indicate that, for $\alpha=5$, 10 and 20, the maximum SNR are obtained when $\beta=0.592$, 1.359 and 2.948, respectively. Fig. 7 shows the relation between the SNR and β taking α as a parameter. As will be seen in the figure, the SNR decreases with the increase of β only slightly, so that the integrator time constant would be better if it were larger. However, this decreases the integrator output, and hence reduces the

For large values of α, (27) is approximately reduced to the following.

$$\frac{S^2}{N^2} = M^2 \frac{3\alpha^5\beta_1^4\gamma^2}{1+\frac{4}{3}\pi^2(1+\gamma^2)\beta_1^2+\frac{16}{5}\pi^4\beta_1^4\gamma^2}. \quad (30)$$

This indicates that the SNR is proportional to $(f_r)^{5/2}$.

Figs. 9 and 10 show the calculated SNR vs γ taking α and β_1 as parameters. The figures indicate that the SNR is constant if either one of β_1 and β_2 is sufficiently large and that the SNR is maximum at an optimum value of γ but does not decrease appreciably if γ exceeds the optimum value.

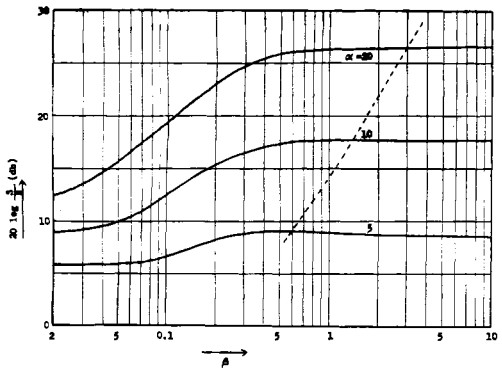

Fig. 7—Theoretical SNR vs normalized integrator time constant β taking the normalized sampling frequency α as the parameter.

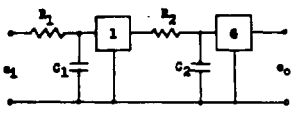

Fig. 8—Double integrator.

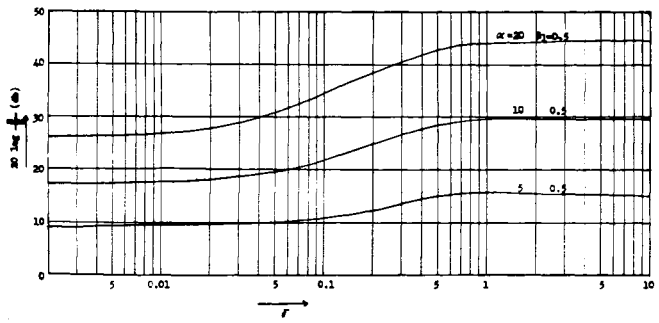

Fig. 9—Theoretical SNR vs the ratio of integrator time constants γ taking normalized time constant β_1 and normalized sampling frequency α as parameters (double integrator).

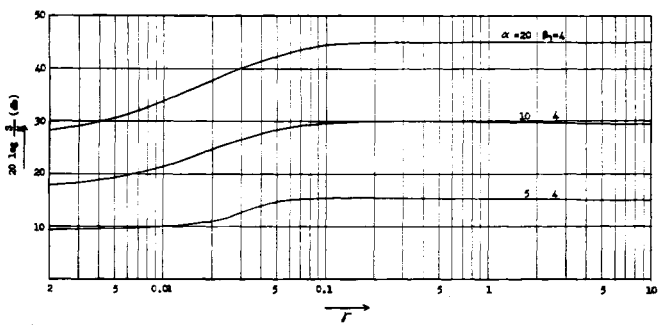

Fig. 10—Theoretical SNR vs the ratio of integrator time constants γ taking normalized time constant β_1 and normalized sampling frequency α as parameters (double integrator).

SNR and Signal Amplitude

The SNR of the system is maximum at an optimum signal amplitude. This is due to the fact that when the signal amplitude approaches from the center to the lower or the upper edge of the dynamic range, the equivalent repetition frequency of the output pulse reduces. Assuming that the repetition frequency reduces linearly with the departure of the signal amplitude from the center of the dynamic range, the equivalent normalized repetition frequency α is

$$\alpha = \alpha_0\left(1 - \frac{|s|}{h}\right) \tag{31}$$

where α_0 is the normalized repetition frequency when the signal amplitude is in the center of the dynamic range and s is the instantaneous signal amplitude. Assuming also that the probability of the input signal taking the amplitude between $|s|$ and $|s+ds|$ as $p(s)ds$, the quantizing noise power increases by the following factor H.

$$H = 2\int_0^{s_0}\left(1 - \frac{s}{h}\right)^{-2k-1} p(s)ds \tag{32}$$

where s_0 is the maximum signal amplitude and k takes the value of one for single integration and two for double integration, respectively.

Now, provided that the input signal has a uniform probability density of amplitude such as a triangular waveform, $p(s) = 1/2s_0$ and the above equation is easily integrated to reduce to the following equation.

$$H = \frac{M(1 - M)^{2k}}{1 - (1 - M)^{2k}}. \tag{33}$$

Taking this factor into consideration, the calculated SNR vs M for $k=1$, $\beta=\infty$, $\alpha_0=20$ is shown in Fig. 11. When the input signal is sinusoidal, it is impossible to express H as a simple function of M. But the results of numerical calculations reveal that the SNR vs M curve for a sinusoidal input is not too different from that of a triangular input.

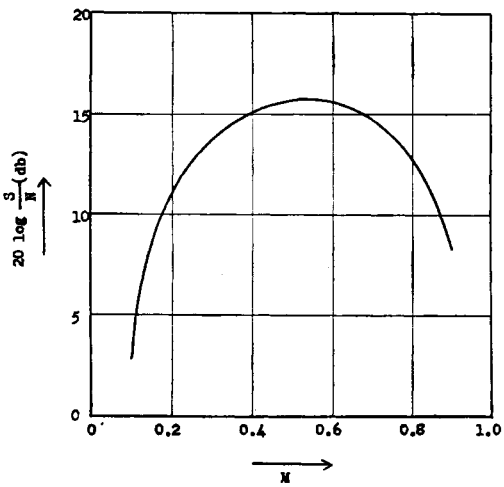

Fig. 11—Theoretical SNR vs normalized signal amplitude.

Periodic Noise

This modulation system is subject to another sort of noise, that is, periodic noise which depends on the levels of dc input signal.

The aspects of generation of periodic noise are simply explained as follows. The modulation may be considered

to be a sort of density modulation, if the output pulses are observed for a considerably long time. Therefore, the density d of output pulses corresponds to the input signal amplitude.

Putting d and f_d as the density and the fundamental frequency of the output pulses, respectively, when the input signal amplitude is s,

$$d = \frac{1}{2}\left(1 - \frac{s}{h}\right) \tag{34}$$

and

$$f_d = \frac{1}{2}\left(1 - \frac{s}{h}\right) f_r \tag{35}$$

where the definition of s, h, f_r is the same as in the previous sections.

If we assume that the distribution of pulses in a period $T_d = 1/f_d$ is as shown in Fig. 12, the series of pulses $P_d(t)$ is expressed as follows.

$$P_d(t) = hd + \frac{2h}{\pi}\sum_{n=1}^{\infty}\frac{1}{n}\sin n\pi d \cos 2\pi n f_d t. \tag{36}$$

Hence the amplitude A_1 of the fundamental component of $P_d(t)$ normalized by h is

$$A_1 = \frac{2}{\pi}\sin \pi d. \tag{37}$$

The periodic component of $P_d(t)$ appears in the demodulated output when the fundamental frequency f_d becomes equal to or smaller than the cutoff frequency f_c of the low-pass filter.

Putting $f_d = f_c$, $d = f_c/f_r = 1/\alpha$. Then, (43) becomes

$$A_1 = \frac{2}{\pi}\sin\frac{\pi}{\alpha}. \tag{38}$$

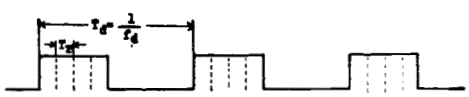

Fig. 12—An example of periodic output pulses.

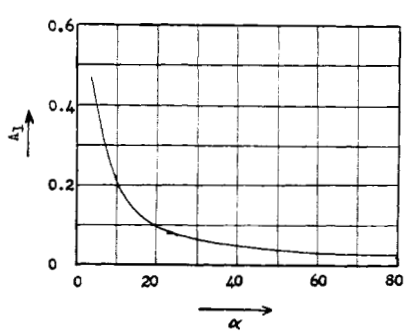

Fig. 13—Fundamental component of periodic noise vs normalized pulse repetition frequency α.

Fig. 13 show the relation between A_1 and α.

Periodic noise becomes comparable with quantizing noise when α is small.

Experimental Results on System Characteristics

Experimental equipment has been constructed to show the realizability of the principle. In order to be compared with the results of the theoretical calculations, the experimental characteristics will be described which have been obtained by the equipment having the signal bandwidth of dc to 4 kc and the variable sampling frequency from 10 kc to 500 kc. Fig. 14 shows the block diagram of the equipment.

Input-Output Characteristics

Fig. 15 indicates the over-all input-output characteristics with dc input showing appreciable linearity. Characteristics to the sinusoidal inputs are essentially the same.

Frequency Characteristics

Fig. 16 shows the over-all frequency characteristics of the modulation system compared with the low-pass filter in the demodulator. The similarity of both curves suggests that the frequency characteristics of the system itself may be independent of the signal frequency.

Signal-to-Quantizing-Noise Ratio

Fig. 17 shows the measured SNR of the system with a single integrator against the pulse repetition frequency taking the signal frequency as the parameter. It can be seen that SNR is improved by the rate of 9 db/oct as the theoretical calculations indicate.

Fig. 18 shows the relation between the measured SNR of the system with a single integrator and the signal frequency. The dependence of the SNR on signal frequency may be considered to be resulted from the characteristics of the low-pass filter so that the SNR of the modulation system itself may be taken as independent of the signal frequency.

Fig. 19 shows the measured SNR of the system with single integration against integrator time constant, taking pulse repetition frequency as a parameter. As the theory of the previous section predicts, there exists the optimum value of time constant.

Fig. 20 (p. 1531) is an example of the measured SNR of the system with single integration against the signal amplitude. The SNR has a certain maximum as has been shown by the calculation.

Fig. 21 shows the measured SNR of the system with double integration against the pulse repetition frequency. Since the time constants of the experimental integrators have been chosen smaller than the optimum value, the absolute value of the SNR is smaller, but the figure shows that the SNR improvement rate with respect to the pulse repetition frequency is 15 db/oct which conforms well to the theoretical calculation.

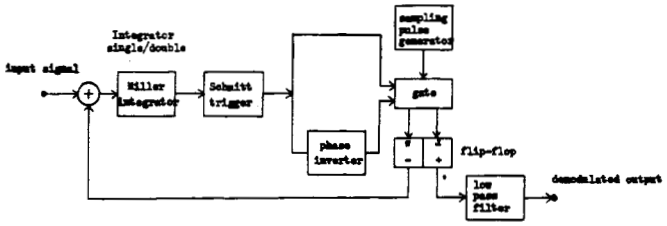

Fig. 14—Block diagram of the experimental modulation system.

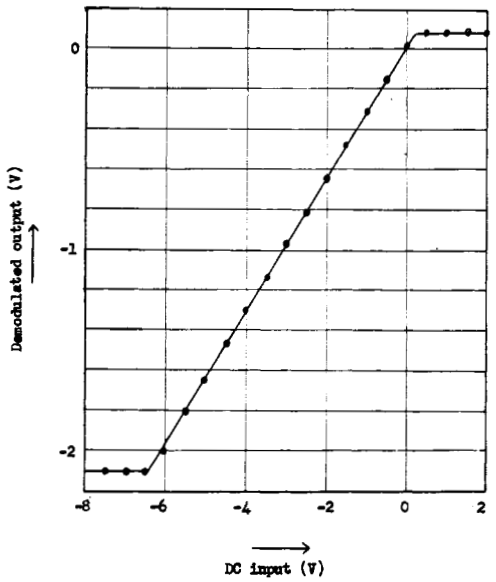

Fig. 15—Input-output characteristics (dc input).

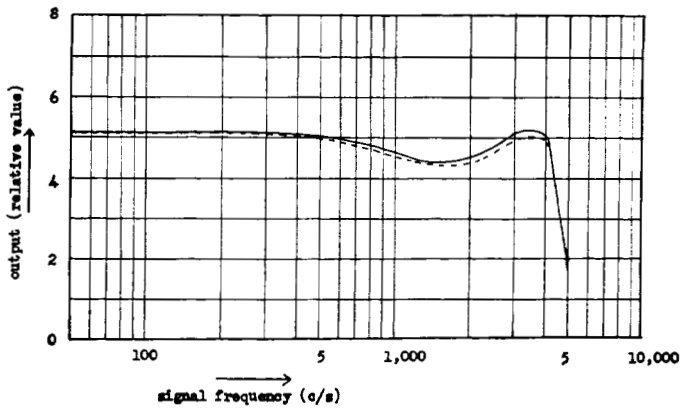

Fig. 16—Frequency characteristic of the experimental equipment.

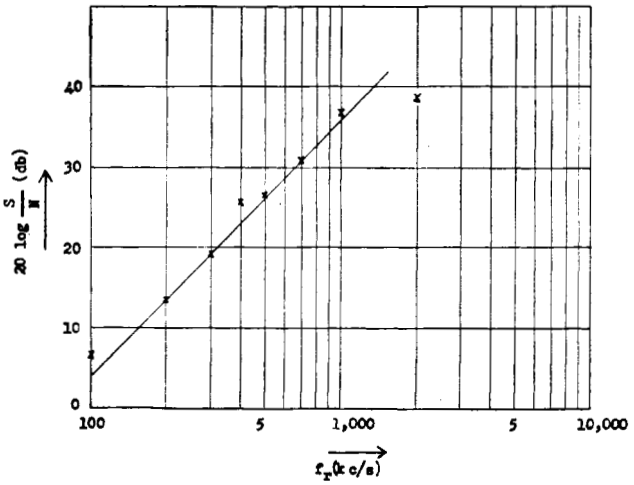

Fig. 17—Measured SNR vs pulse repetition frequency.

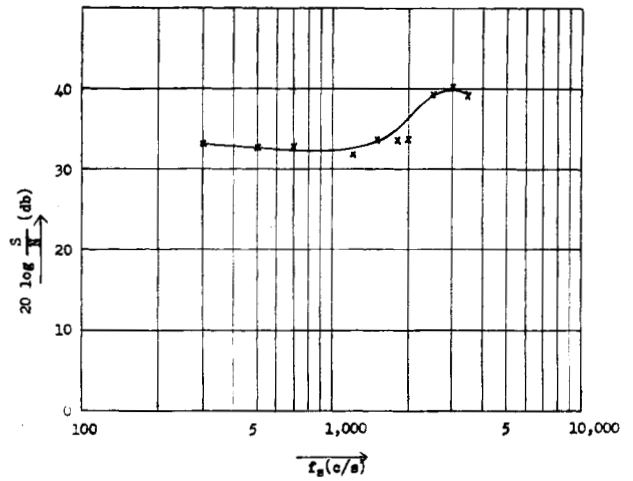

Fig. 18—Measured SNR vs signal frequency.

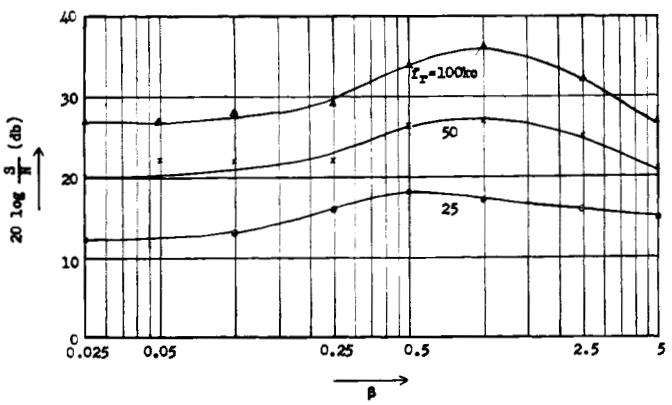

Fig. 19—Measured SNR vs noramlized integrator time constant β.

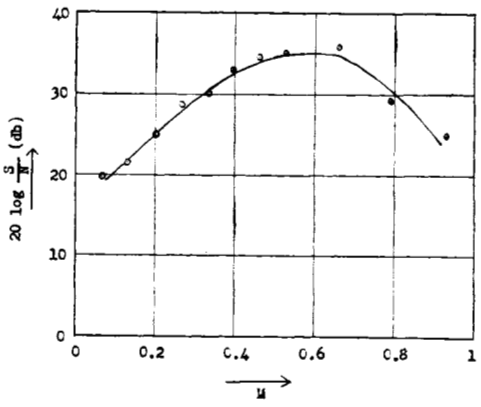

Fig. 20—Measured SNR vs normalized signal amplitude M.

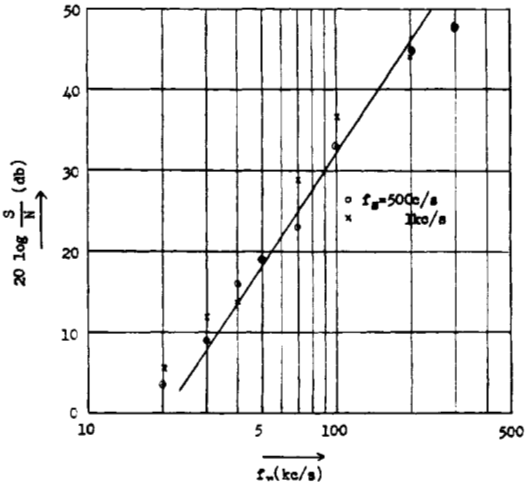

Fig. 21—Measured SNR vs pulse repetition frequency (double integration).

Coding of Video Signals—An Example of the System

PCM[3–5] and delta modulation[6] techniques have been applied to the digital transmission of video signals. The PCM video encoder is considerably expensive and complicated because of the inevitable use of coding tubes or parallel coding arrangements. The application of the delta modulation to the video encoding simplifies circuitry and keeps the naturalness of the demodulated picture especially at low sampling rates.

The proposed system which possesses, in addition to the above mentioned features of delta modulation, such advantages that the dynamic range as well as SNR are independent of the signal frequency, may be considered to fit the purpose in view of the fact that the video signals have frequency spectra extending rather uniformly from very low frequency to a few megacycles. The design and characteristics of a video encoder are described here as examples of the experimental systems which have been constructed to demonstrate the feasibility of the principle.

Figs. 22 and 23 show schematically the basic composition and waveforms of the encoder. An Esaki diode is preferred as the pulse modulator. As shown in Fig. 24, the "set" and "reset" points of the Esaki diode are determined by the load line which is decided by the resistors R_a, R_b, R_c, R_d and the supply voltage. Assuming that the Esaki diode is in the "reset" state, when the input signal $s(t)$ increases, the output of the integrator raises the load line upward. Thus a sampling pulse of positive polarity switches the Esaki diode to the "set" state. As the result, the current through the Esaki diode reduces and the potential drop across the resistor R_a decreases. This is fed back to the input so that the increase of the input signal level is reduced. The Esaki diode is then reset by a succeeding sampling pulse of negative polarity. In other words, the resultant output $-p(t)$ of the Esaki diode is added to the input signal $s(t)$. The integrator integrates the signal $s(t)-p(t)$ and feeds the integrated difference signal $\epsilon(t)=\int\{s(t)-p(t)\}dt$ to the pulse modulator. If $\epsilon(t)$ is larger than the trigger level, the Esaki diode is switched again and reduces $\epsilon(t)$. If not, the Esaki diode remains unswitched. Through this negative feedback procedure, the integrated difference signal is always kept in the vicinity of the reference level at which the Esaki diode is triggered. Thus the output of the Esaki diode carries the information corresponding to the instantaneous amplitude of the input signal. The circuit is considerably simplified by using an Esaki diode. This is essential to reduce the circuit delay as well as the power consumption.

Although the principle of operation is described in the case that the comparison is performed at the "reset" state of the Esaki diode, the operation can be performed at the "set" state as well. In this case the Esaki diode provides output pulse $p(t)$ of positive polarity.

Figs. 25 and 26 show the modulator and demodulator circuits of the experimental system, respectively. The input of the modulator and the output of the demodulator are terminated by 75-Ω resistors. The dynamic range of the modulator is designed to be 75 mv, so that the video signal input of approximately 1 volt is divided by 20 and fed to the modulator. In the experimental system, the output of the modulator is directly connected to the demodulator through an emitter follower.

The modulator is composed of a summing network, a high-frequency amplifier, an integrator and a pulse modulator. The high-frequency amplifier is provided to

[3] W. M. Goodall, "Pulse code modulation for television," *Bell Lab. Record*, vol. 29, pp. 209–211; May, 1951.
[4] R. L. Carbrey, "Video transmission over telephone cable pairs by pulse code modulation," Proc. IRE, vol. 48, pp. 1546–1561; September, 1960.
[5] S. Oshima, H. Enomoto, and K. Amano, "High-speed logic circuit using Esaki diode," *J. Inst. Elec. Commun. Engrs.* of Japan, vol. 45, pp. 1541–1548; November, 1962.
[6] J. C. Balder and C. Kramer, "Video transmission by delta modulation using tunnel diodes," Proc. IRE, vol. 50, pp. 428–431; April, 1962.

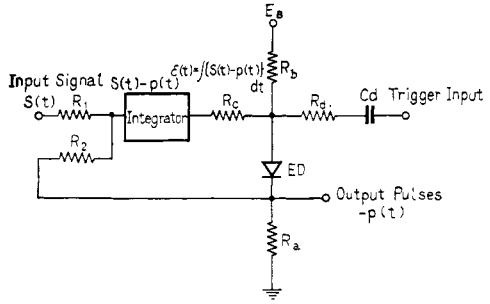

Fig. 22—Basic composition of the encoder.

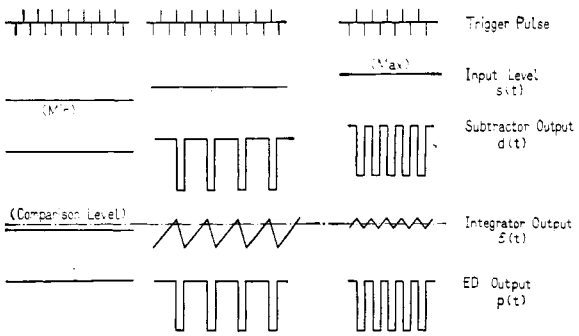

Fig. 23—Schematic waveforms of the encoder.

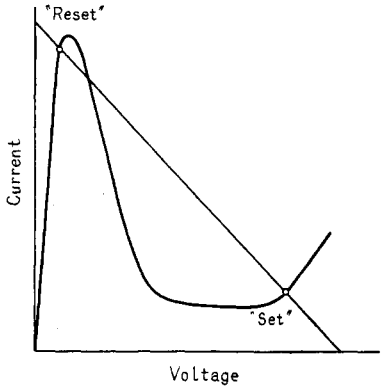

Fig. 24—Operating points of the Esaki diode comparator.

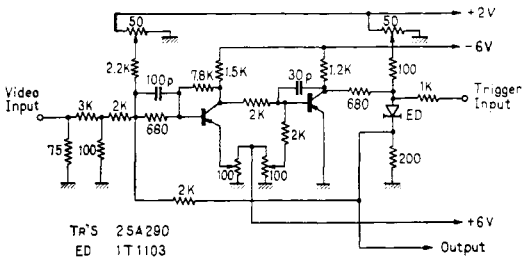

Fig. 25—Experimental modulator circuitry.

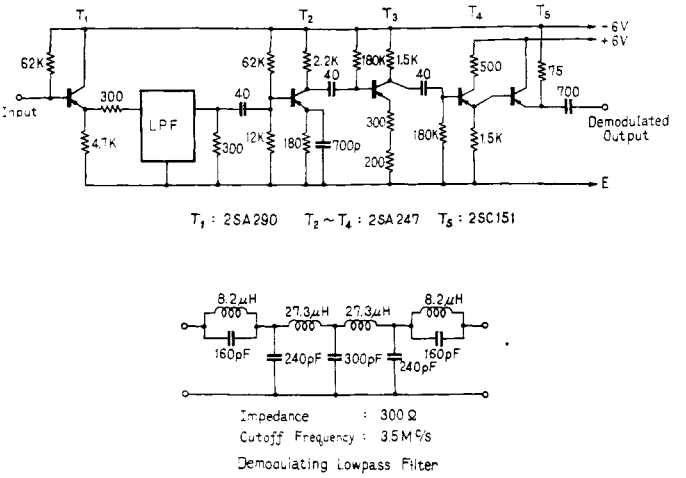

Fig. 26—Experimental demodulator circuitry.

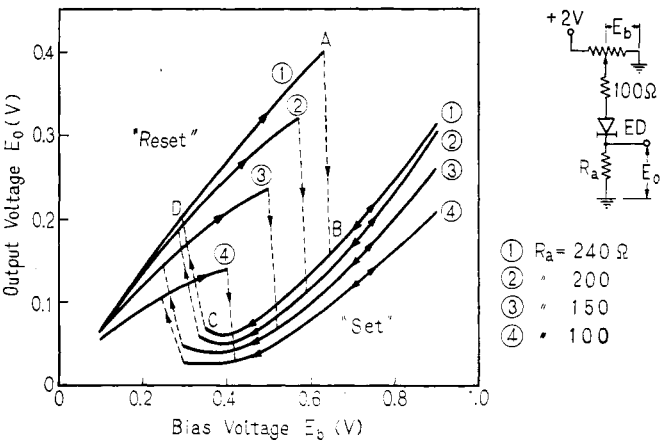

Fig. 27—dc characteristics of the comparator.

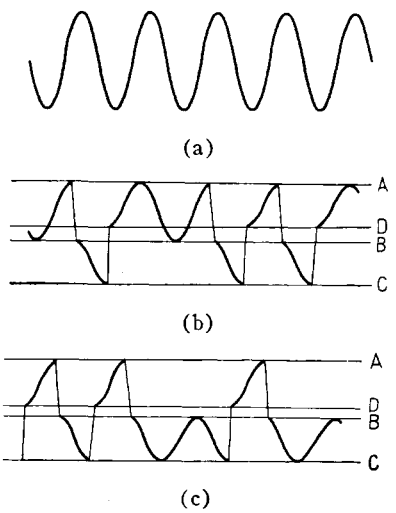

Fig. 28—Trigger and output waveforms. (a) Sinusoidal trigger. (b Output waveform comparison at A (negative output). (c) Output waveform comparison at C (positive output).

amplify the output of the summing network in order to have sufficient output level of the integrator to trigger the Esaki diode. The amplifier should have enough bandwidth to deal with signals with the repetition frequency of sampling pulses. Employing negative feedback and peaking as shown, a common emitter amplifier with the transistor 2SA290 ($f_\alpha = 700$ Mc) has been constructed. The bandwidth and the gain of the amplifier are 0 to 50 Mc and 9, respectively. The integrator is a Miller integrator composed of a transistor 2SA290, a 2-kΩ resistor and a 30-pf capacitor. The frequency characteristics of the integrator have been proved satisfactory over the operating frequency range.

An Esaki diode 1T1103 with peak current of 2 ma, valley current of 0.3 ma, peak voltage of 40 mv, valley voltage of 300 mv and capacity of 6 pf, has been employed for the pulse modulator. Experiments have been carried out to choose optimum values of resistors so as to have larger output voltage with tolerable distortion of output waveforms. Fig. 27 shows the dc characteristics of the comparator. Figs. 28(b) and (c) show the output waveforms when triggered by sinusoidal wave of Fig. 28(a). The waveform of Fig. 28 (b) is obtained when the comparison level is chosen at point A in Fig. 27, which corresponds to the "reset" point in Fig. 24. Assuming that the Esaki diode is in set state when the negative trigger exceeds point C, the Esaki diode is reset and jumps to point D. The circuit parameters are chosen so that the jump occurs at the negative peak. Following this the output waveform moves from point D to point A according to the increase of the trigger amplitude. At point A, if the integrator output voltage plus trigger amplitude is more than the voltage of point A, the Esaki diode is set and jumps to point B. The waveform of Fig. 27(b) results from this procedure and the negative output pulse is identified to be present when the waveform exceeds the level B, so that the voltage between C and B should preferably be made larger than the voltage between B and A. The waveform of Fig. 28(c) is obtained when the comparison level is chosen at point C in Fig. 27 which corresponds to the "set" point in Fig. 24. The polarity of output pulse is positive in this case. In the experimental system, the positive output resulted from the comparison at point C is preferred because the output amplitude is larger.

The demodulator consists of a low-pass filter and a transitor amplifier. The low-pass filter has been designed to have the cutoff frequency of 4 Mc.

Fig. 29 shows the input-output characteristics of the experimental system for the signal frequency of 1 Mc and for the sampling frequency of 40 Mc. Fig. 30 shows the over-all frequency characteristics of the system. Figs. 31 (a), (b), (c), (d) and (e), on page 1534, show the output waveform of the modulator with dc input at the sampling rate of 10 Mc to 50 Mc. Fig. 32 (a) shows 500-kc sinusoidal input to the modulator and Figs. 32 (b), (c), (d), (e) and (f) show the demodulator output waveforms at the sampling rate of 10 Mc to 50 Mc.

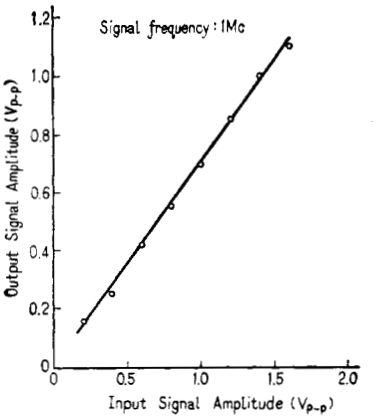

Fig. 29—Input-output characteristics of the experimental system.

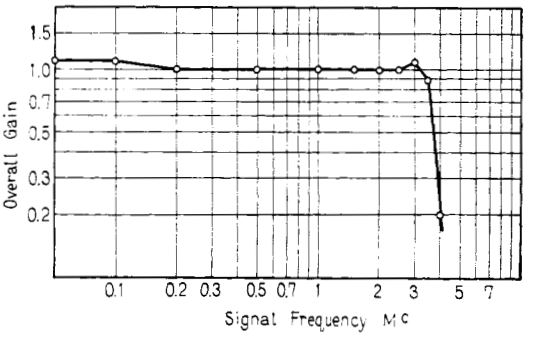

Fig. 30—Over-all frequency characteristics.

Feeding standard test pattern signals to the experimental system, demodulated signals have been displayed on a television monitor. Fig. 33 (a) shows the original test pattern and Figs. 33 (b), (c), (d), (e) and (f) show the demodulated pattern at the sampling rate of 10 Mc to 50 Mc. The result of observations indicates that the system operating at the sampling rate as low as 30 Mc reproduces a considerably good picture and that even at the sampling rate of 10 Mc the reproduction is better than 1-bit PCM.

Acknowledgment

Thanks are due to Professor Sakamoto and the members of the Laboratory of the University of Tokyo for their advice, and to J. Murakami, H. Fujita and H. Takano for their experimental contributions.

The authors also wish to acknowledge with thanks the grant of the High Speed PCM Research Project of the Ministry of Education under the direction of Professor T. Osatake, the supports of Dr. I. Sikiguchi of the Central Research Laboratories, Hitachi Limited and the Okabe Memorial Scholarship of the Institute of Electrical Communication Engineers of Japan.

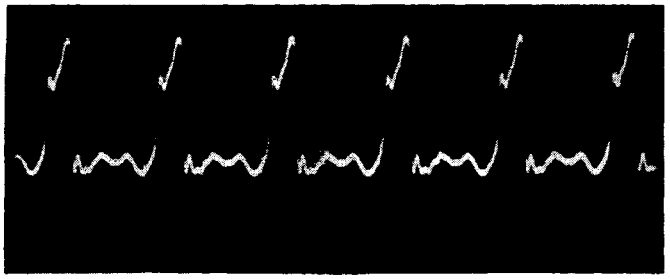

(a)

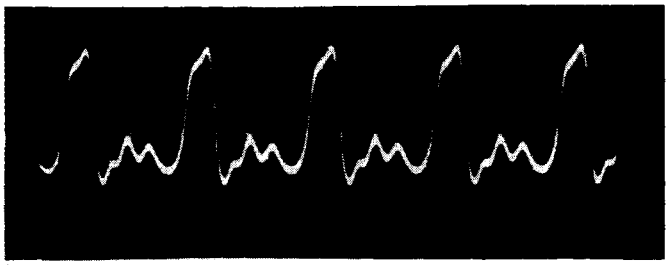

(b)

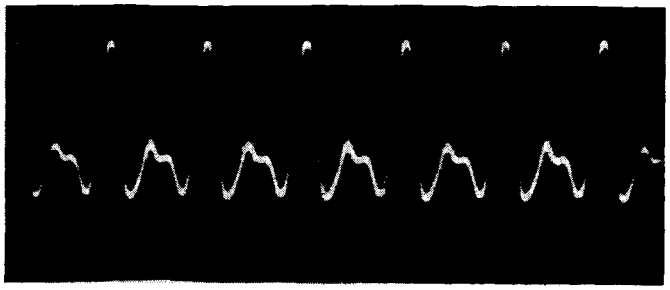

(c)

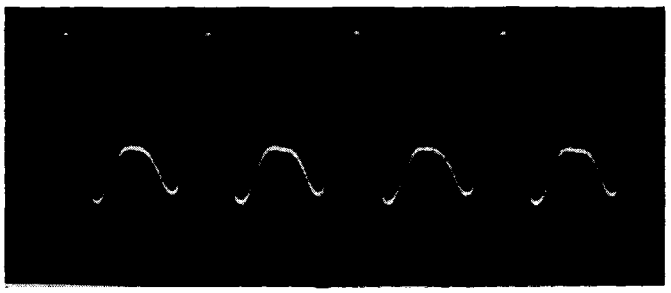

(d)

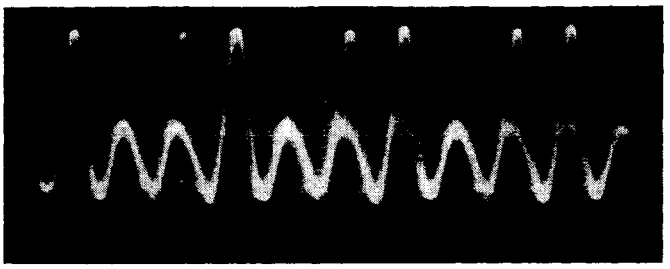

(e)

Fig. 31—(a) $f_r = 10$ Mc, H: 0.04 μsec/d.v., V: 0.1 v/d.v. (b) $f_r = 20$ Mc, H: 0.04 μsec/d.v., V: 0.1 v/d.v. (c) $f_r = 30$ Mc, H: 0.04 μsec/d.v., V: 0.1 v/d.v. (d) $f_r = 40$ Mc, H: 0.02 μsec/d.v., V: 0.1 v/d.v. (e) $f_r = 50$ Mc, H: 0.02 μsec/d.v., V: 0.1 v/d.v.

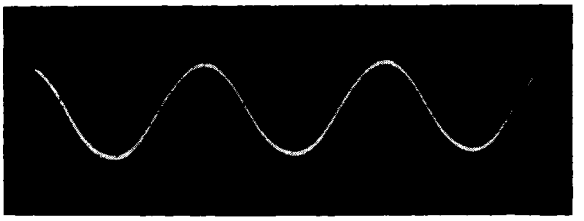

(a)

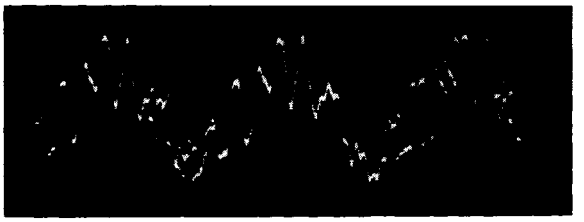

(b)

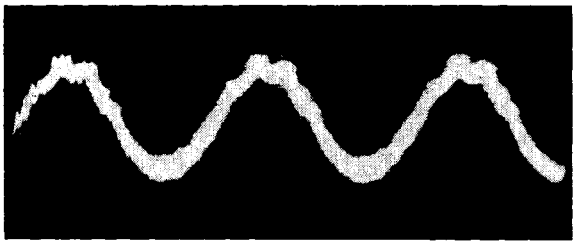

(c)

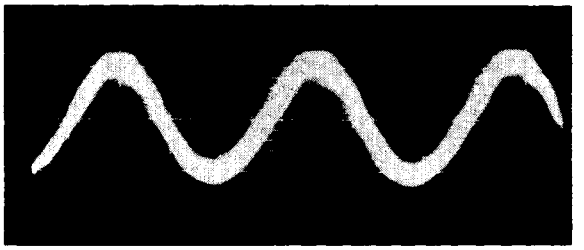

(d)

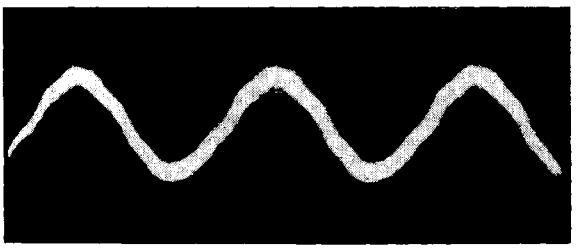

(e)

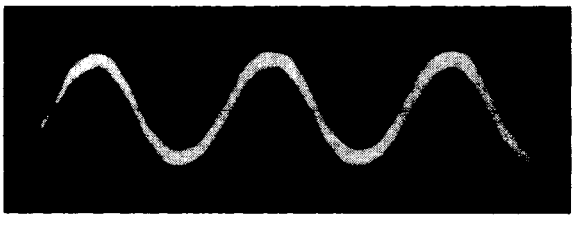

(f)

Fig. 32—(a) Input: 500 kc sinusoid, H: 0.5 μsec/d.v., V: 0.5 v/d.v. (b) f_r: 10 Mc, H: 0.5 μsec/d.v., V: 0.5 v/d.v. (c) f_r: 20 Mc, H: 0.5 μsec/d.v., V: 0.5 v/d.v. (d) f_r: 30 Mc, H: 0.5 μsec/d.v., V: 0.5 v d.v. (e) f_f: 40 Mc, H: 0.5 μsec/d.v., : V 0.5 v d.v. (f) f_r: 50 Mc, H: 0.5 μsec/d.v., V: 0.5 v d.v.

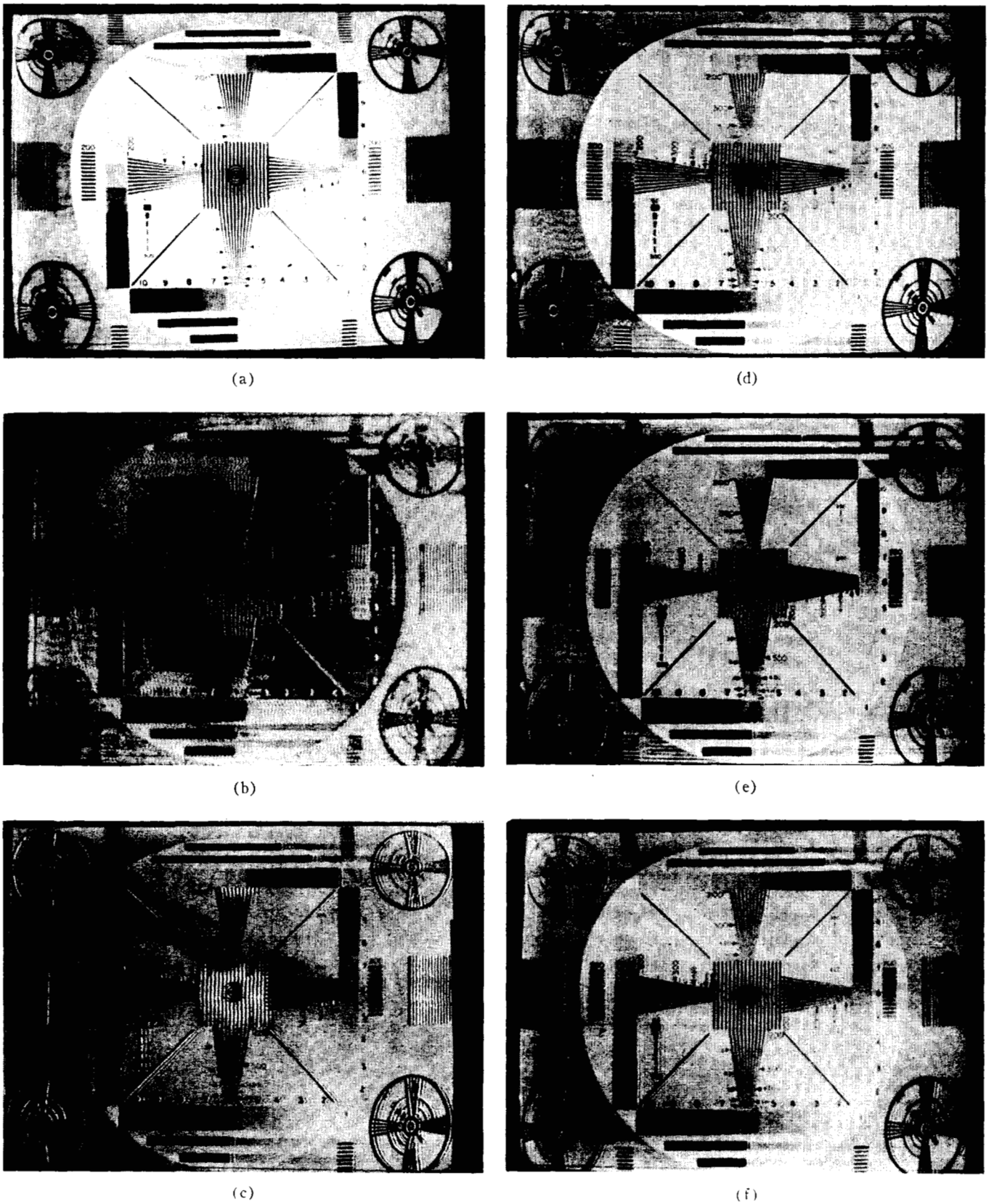

(a) (d)

(b) (e)

(c) (f)

Fig. 33— (a) Original. (b) $f_r = 10$ Mc. (c) $f_r = 20$ Mc. (d) $f_r = 30$ Mc. (e) $f_r = 40$ Mc. (f) $f_r = 50$ Mc.

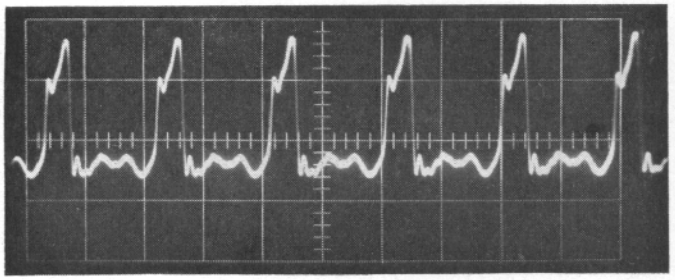

(a)

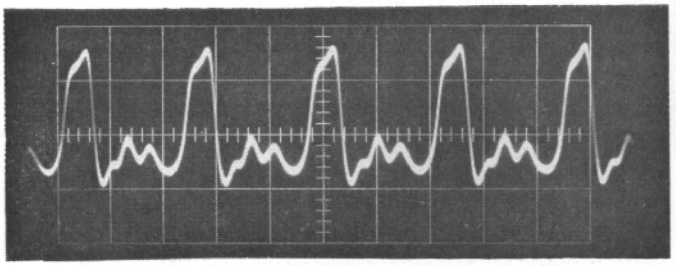

(b)

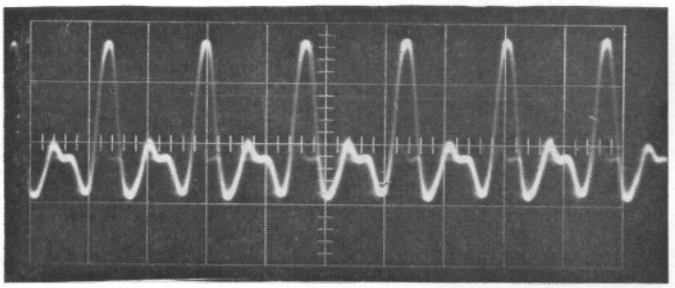

(c)

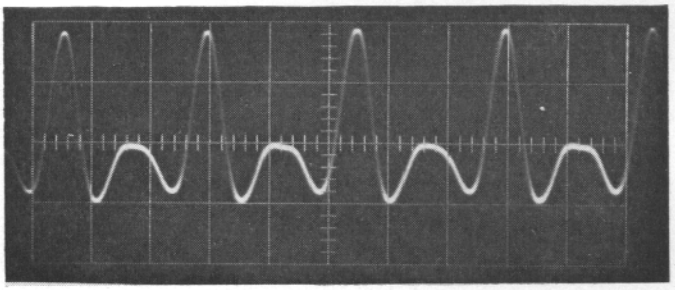

(d)

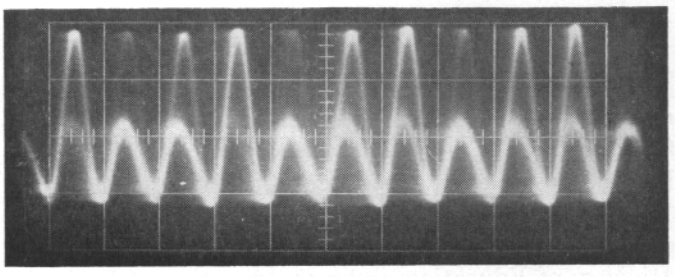

(e)

Fig. 31—(a) $f_r = 10$ Mc, H: 0.04 μsec/d.v., V: 0.1 v/d.v. (b) $f_r = 20$ Mc, H: 0.04 μsec/d.v., V: 0.1 v/d.v. (c) $f_r = 30$ Mc, H: 0.04 μsec/d.v., V: 0.1 v/d.v. (d) $f_r = 40$ Mc, H: 0.02 μsec/d.v., V: 0.1 v/d.v. (e) $f_r = 50$ Mc, H: 0.02 μsec/d.v., V: 0.1 v/d.v.

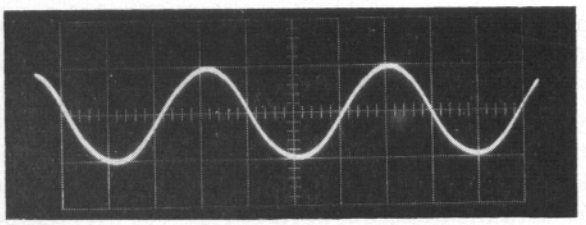

(a)

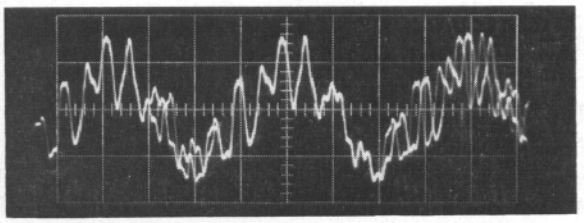

(b)

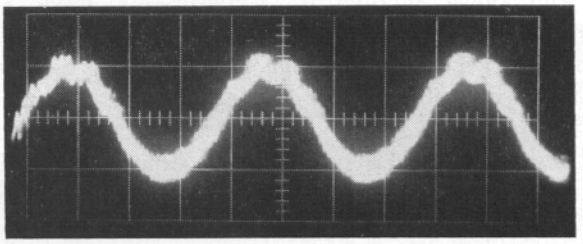

(c)

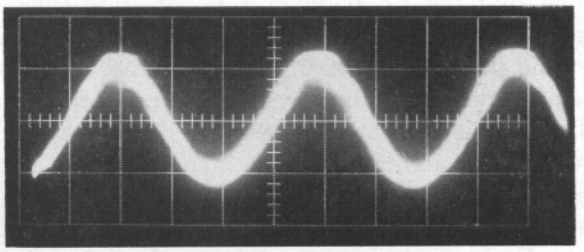

(d)

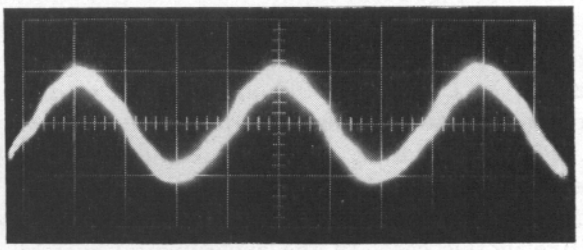

(e)

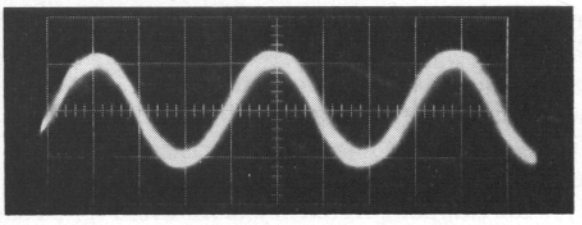

(f)

Fig. 32—(a) Input: 500 kc sinusoid, H: 0.5 μsec/d.v., V: 0.5 v/d.v. (b) f_r: 10 Mc, H: 0.5 μsec/d.v., V: 0.5 v/d.v. (c) f_r: 20 Mc, H: 0.5 μsec/d.v., V: 0.5 v/d.v. (d) f_r: 30 Mc, H: 0.5 μsec/d.v., V: 0.5 v d.v. (e) f_f: 40 Mc, H: 0.5 μsec/d.v., : V 0.5 v d.v. (f) f_r: 50 Mc, H: 0.5 μsec/d.v., V: 0.5 v d.v.

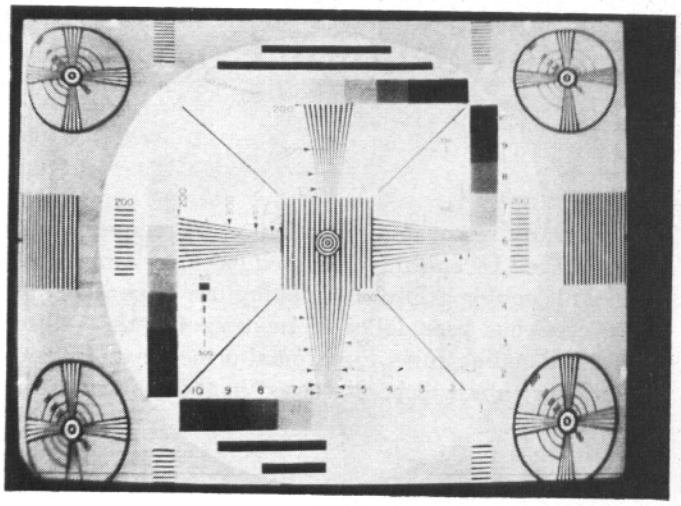

(a)

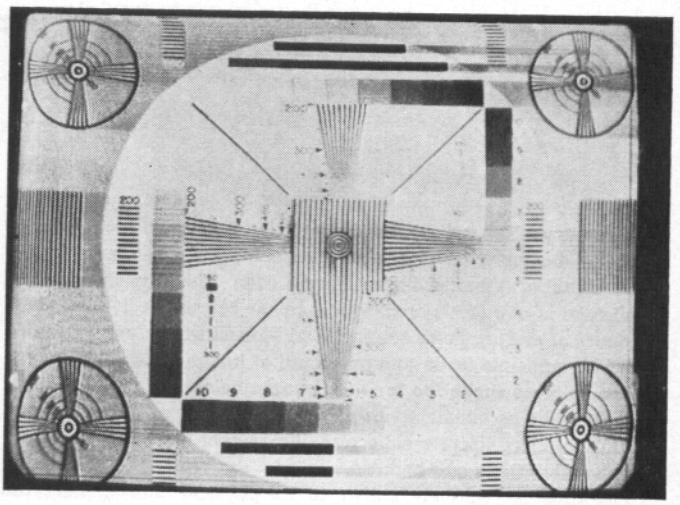

(d)

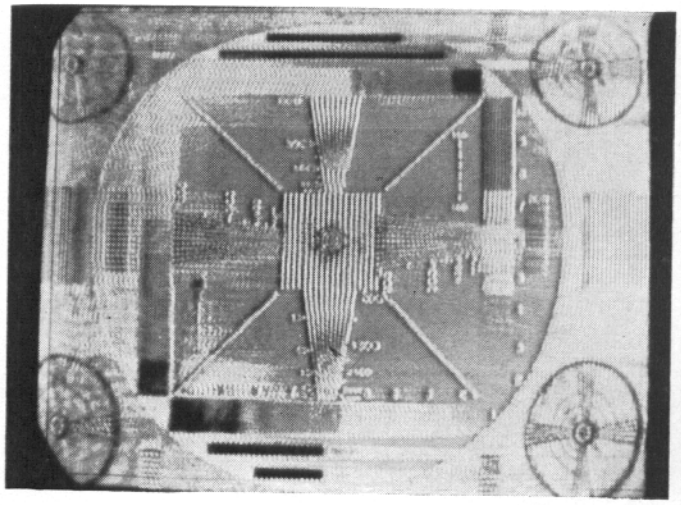

(b)

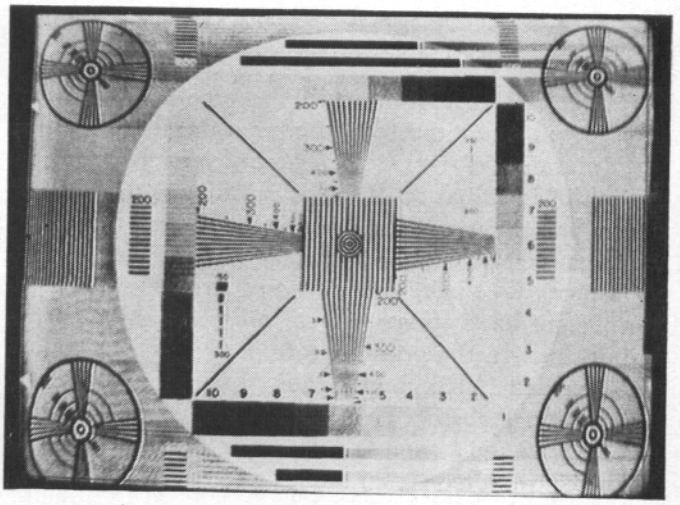

(e)

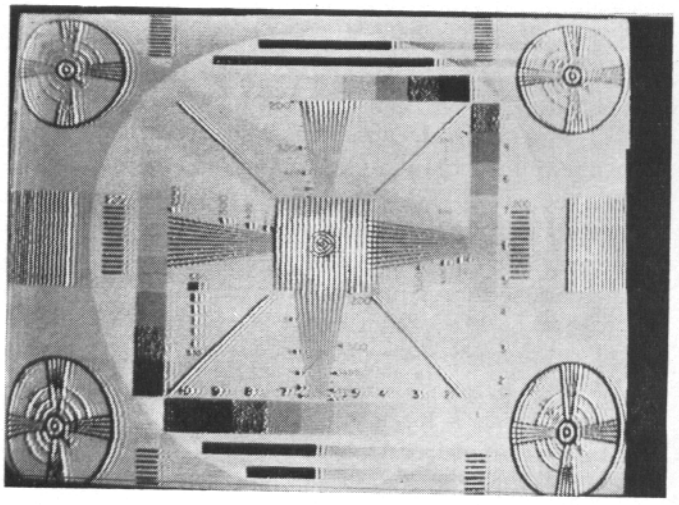

(c)

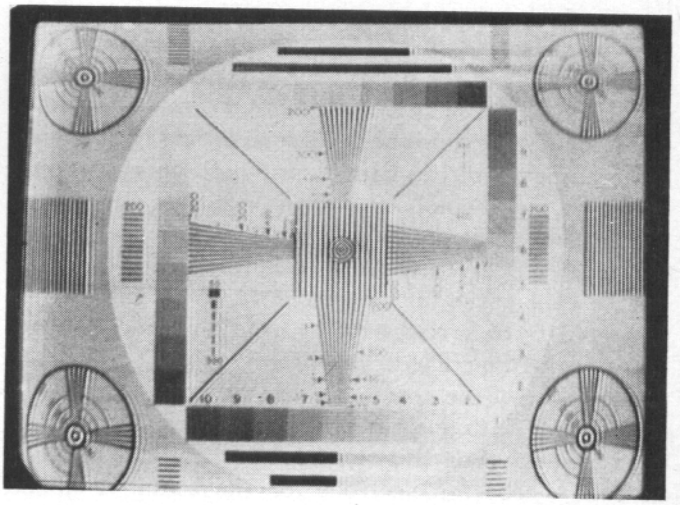

(f)

Fig. 33— (a) Original. (b) $f_r = 10$ Mc. (c) $f_r = 20$ Mc. (d) $f_r = 30$ Mc. (e) $f_r = 40$ Mc. (f) $f_r = 50$ Mc.